High temperature behavior of water inside flat graphite nanochannels

M. C. Gordillo
Departamento de Sistemas Físicos, Químicos y Naturales, Facultad de Ciencias Experimentales, Universidad Pablo de Olavide, Carretera de Utrera, km 1, 41013 Sevilla, Spain

J. Martí
Departament de Física i Enginyeria Nuclear, Universitat Politècnica de Catalunya, B5-206 Campus Nord, 08034 Barcelona, Catalonia, Spain

(Received 27 June 2006; revised manuscript received 22 September 2006; published 6 February 2007)

By means of molecular dynamics calculations performed at high temperatures, we were able to calculate the phase diagram of liquid water confined inside narrow graphite channels. We found stable liquid phases all the way to 398 K, failing to reach the critical temperature for all of the systems under consideration. We also analyzed how the temperature variations in the range of 298 to 398 K affected the hydrogen bond network and found that the main variation in the infrared spectra of confined water at high temperatures was the forward shifting of the bending peak.

DOI: 10.1103/PhysRevB.75.085406 PACS number(s): 68.08.De, 61.30.Hn, 61.20.Qg, 31.15.Qg

I. INTRODUCTION

Molecular dynamics (MD) is a standard technique widely used to investigate properties of water in a variety of conditions, in particular in confined situations. For instance, there is a fair amount of work reporting what happens to water inside slit pores,[1–4] graphite,[5–13] or cylindrical pores.[14–17] When the appropriate potentials are used, MD is reliable enough to allow us to obtain information directly comparable with experiments.[18,19] Its main advantage with respect to other kind of calculations such as Monte Carlo simulations, is that it affords the study of dynamical properties, like infrared (IR) spectra or residence times of the atoms or molecules in a particular place or environment. There is a drawback, however. With MD one cannot, in principle, obtain directly other properties such as thermodynamical stability ranges. This shortage can be amended by the use of indirect methods, like the ones indicated in Ref. 20. Those kinds of calculation allow us to obtain indirectly the free energy of different phases and, from that, to calculate the phase diagram of the systems under consideration. This has been made for water between flat graphite plates,[21,22] but only for low temperature arrangements. The goal of this paper is to extend those simulations to higher temperatures, defining the phase diagram of confined water up to $\sim$125 °C, answering the question of what happens to confined water at high temperatures, something that has been scarcely addressed until now.

The plan of the paper is as follows. In Sec. II we will state the model and the simulation details, while the results are to be described in Sec. III. After that, some conclusions will be given.

II. MODEL AND SIMULATION DETAILS

We studied the high temperature behavior of water confined between two graphite parallel plates with no defects. The z direction was taken to be the one perpendicular to the hydrophobic sheets. Three systems were considered with separation between the graphite layers of 9, 12, and 15 Å. These distances were the shortest ones measured from the center of a carbon to another carbon in the opposite graphite plane. These layers had a surface of 34.4×34.1 Å^2 in all cases and served to model the behavior of an homogeneous infinite system. For these three water arrangements, we performed MD simulations at seven temperatures regularly spaced from 323 to 398 K, in a density range large enough to observe unambiguously the phase separations.

As in previous studies, the water-water inter- and intramolecular interactions were described by a flexible simple point charge (SPC) potential,[23] while water-graphite forces have been assumed to be of the Lennard-Jones type with the same parametrization of previous works (see, for instance, Ref. 14), but considering explicitly all the carbons belonging to the two limiting layers. The SPC model was used because it reproduces accurately the critical temperature of bulk water,[26] the parameters of the flexible version used here being fitted to reproduce the main features of the ir spectra of bulk water at room conditions.[23] Thus, with this model one expects to obtain accurate thermodynamical and dynamical properties for the system under consideration. The customary three-dimensional (3D) Ewald sums were used to account for electrostatic interactions.[24] A leapfrog Verlet integration algorithm with coupling to a thermal bath has also been employed.[25] Our integration time step was 0.5 fs. The runs after equilibration were long enough to assure there were no changes that could affect the results below. That meant runs of 250 ps after equilibration times of 50 ps.

To build the phase diagrams, we had to determine the thermodynamical stability of the simulated systems by means of the Helmholtz free energy F calculations. The free energy was obtained in the same way as in previous studies,[20,21] i.e., by assuming a reasonable expression for F and deriving the corresponding form for the total energy of the system, E, a property of the system directly obtained from the MD simulations. The analytical form for F was taken to be

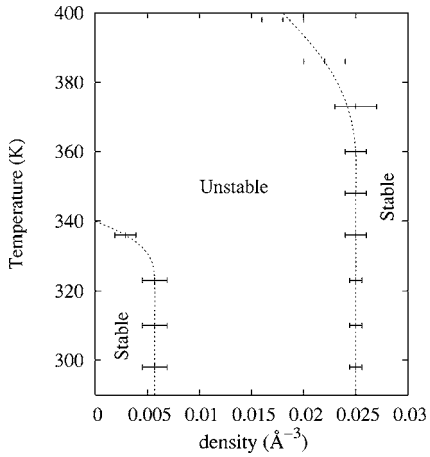

FIG. 1. Phase diagram for the system with 9 Å of interplate separation. Dotted lines are guides to the eye, the crosses with the error bars being the results of our simulations.

$$F(\rho,T) = \sum_{i=0}^{3}\sum_{j=1}^{3} b_{ij}\rho^{i}T^{1-j} + (\text{ideal polyatomic gas terms}). \tag{1}$$

Here, the density ρ was simply the number of molecules divided by the total volume of the simulation cell, the z coordinate being the distance between the center of the carbons discussed above; no allowance was made for the minimum distance between the carbon atoms and the oxygen or hydrogen atoms in the water molecule. For every set of three consecutive temperatures, a fit to the energy derived from the above expression was made, obtaining the thermodynamical stability limits of the phases involved in a considered temperature span (323–398 K). The error bars were obtained for comparison between overlapping ranges. The stability regions below 323 K were taken from Ref. 21, where more details of the entire procedure can be found.

III. RESULTS

Figures 1–3 represent the phase diagrams of water confined between two graphite layers separated by 9, 12, and 15 Å, respectively. In all cases dotted lines are guides to the eye to limit the stable phases. As indicated above, the densities displayed in the abscissas correspond to the total number of water molecules divided by the total space available. From those figures, one can infer the maximum number of water molecules used in each case, by multiplying the volume of the simulation cell by the biggest density displayed for each separation. The "unstable" parts of the figures indicate the densities in which the existence of water is impossible: if we tried to create a phase with that number of molecules in the given space, it would separate in two parts whose densities would correspond to the dotted lines of the figures at the considered temperature. In the cases in which there is only one such dotted line, the system will leave the appropriate empty space to allow the remaining molecules to have adequate density in the limit of the stable range. In the 9 Å case, we observe that the low density stable phase defined in Ref. 21 disappears at temperatures above 340 K, while the high density one increases appreciably its range of stability from the 360 K isotherm up. In any case, we do not see a stable gas phase of appreciable density at high temperatures, meaning that 400 K is still well below the critical temperature for this system. For the sake of comparison, the bulk critical temperature for this model of water is around 640 K,[26] almost identical to the one found experimentally. The remaining two figures are similar in the sense that there exists only a high density stable phase in both of them. However, in the 12 Å diagram, the stability range increases with temperature, being almost constant for the 15 Å separation. In any case, the highest temperature in this study is still short of the critical isotherm for the two wider arrangements.

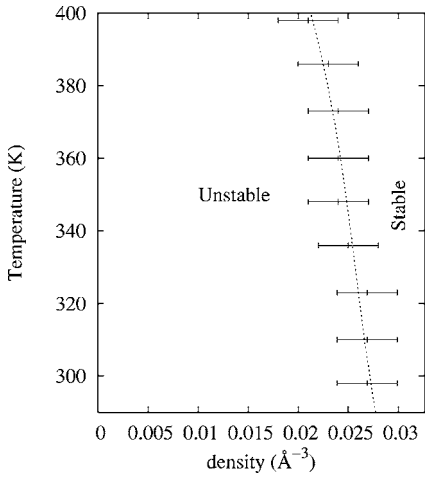

FIG. 2. Same as in Fig. 1 but for a separation 12 Å.

Apart from the definition of the phase diagrams themselves, one could ask how temperature affects the properties of the systems under consideration at a given density inside the stable regimes. To extend the comparison further, we took into account the same effective density for all separations, 5.6×10^{-2} Å^{-3}. This last density was obtained by dividing the number of water molecules by the available space for their centers of mass, i.e., taking into account the fact that the atoms in a water molecule cannot be located at less than

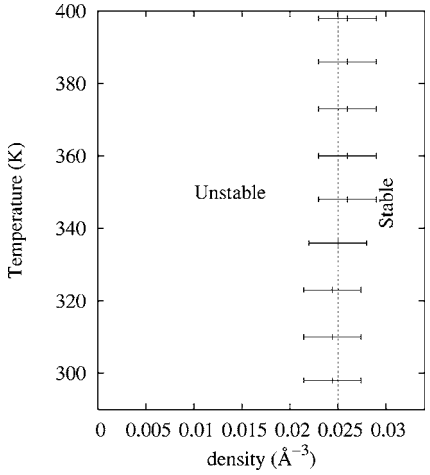

FIG. 3. Same as in previous figures for a slab width of 15 Å.

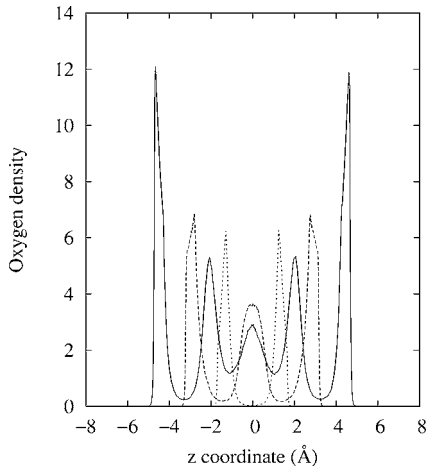

FIG. 4. Oxygen density in g/cm^3 versus the z coordinate for separations 15 (full line), 12 (dashed line) and 9 Å (dotted line). All the data are given at 398 K.

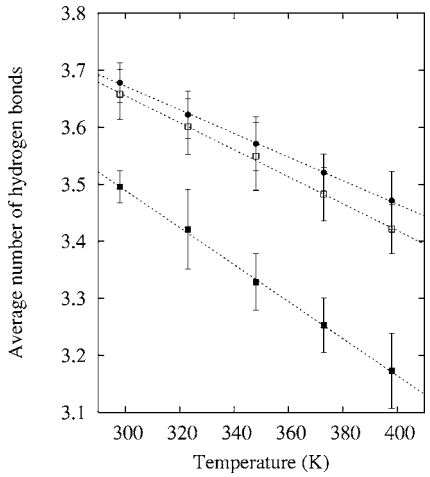

FIG. 5. Average number of hydrogen bonds for the three systems considered: 15 (full circles), 12 (open squares), 9 Å (full squares). Dotted lines are guides to the eye. The destruction rate is shown to depend on the graphite separation.

a certain distance from the center of any carbon in the graphite sheets. Allowing for that space subtraction, the common density corresponds to 2.5×10^{-2} Å^{-3} for the 9 Å separation, 3.3×10^{-2} Å^{-3} in the 12 Å setup, and 3.7×10^{-2} Å^{-3} for the 15 Å arrangement in the units in which the phase diagrams are given. Those densities are in all cases inside the water stability range, and are used to discuss the variation of the structural and dynamical properties explained below.

The first thing one might want to know is how the variations in temperature modify the density profile of water between the two graphite plates. The answer can be deduced with the help of Fig. 4. There, we display the oxygen density profiles (very similar to the center-of-mass densities) for the three z separations considered in this work. The center of the simulation cell was taken to be at the $z=0$ position. In this figure, we represent those profiles at 398 K, the highest temperature of our calculations, finding than they are virtually identical to the same densities at 298 K displayed in Ref. 21. This means that, at least in this range, the overall atom distributions do not change appreciably.

However, this does not mean that the temperature does not affect the structure of the systems at all. In Fig. 5, we can see the evolution of the average number of hydrogen bonds in the three systems considered in this work: from top to bottom, 15, 12, and 9 Å. Here, we incorporated data for 298 K for all the systems under consideration. Two facts are immediately apparent: the number of hydrogen bonds decreases with temperature, and that decrease is proportionally greater in the case of narrower environments. That can be seen through the slopes of the dotted lines which serve as guides to the eye: the wider the z separation, the smaller the slope (~5% in the 15 Å case against ~9% in the 9 Å one). Thus, for wider systems at the same density, one would expect a rate of hydrogen bond destruction very similar to that of a bulk system at the same effective density.

Among the most important dynamical properties of water available through MD simulations are self-diffusion coefficients and spectral densities. Both are related to single-atom velocity autocorrelation functions $C(t)$:

$$C(t)=\frac{\langle\vec{v}(t)\cdot\vec{v}(0)\rangle}{\langle v(0)^2\rangle} \tag{2}$$

where $\vec{v}(t)$ is the velocity of a given atom (oxygen or hydrogen) at time t. The diffusion coefficients D have the expression

$$D_\alpha=\int_0^\infty C(t)_\alpha dt. \tag{3}$$

Here, α stands for the x, y, or z direction. The total self-diffusion average coefficient

$$D=\frac{1}{3}(D_x+D_y+D_z). \tag{4}$$

On the other hand, the spectral densities $S(\omega)$ are calculated by means of the following:

$$S(\omega)=\int_0^\infty C(t)\cos(\omega t)dt. \tag{5}$$

The spectral densities for hydrogen atoms are closely related to the ir spectra, in such a way that only the positions of the peaks of $S(\omega)$ are meaningful and can be compared with experiment.[27,28]

In Fig. 6 we show the result of performing the Fourier-transform technique implied in Eq. (5). From bottom to top we display bulk (density, 1 g/cm^3), z=9, 12, and 15 Å spectra, in all cases at 398 K, the highest temperature in our study. We observe that the spectral densities are very similar to each other and to the bulk case, the main difference being the low frequency peak located at around 50 cm^{-1}, which shifted to around 100 cm^{-1} for the 9 Å case and is a mere shoulder in for the other two separations. This particular feature is basically related to intermolecular vibrations. A detailed description of these intermolecular movements involves the study of additional dynamical properties such as the times of residence of water in particular locations and the

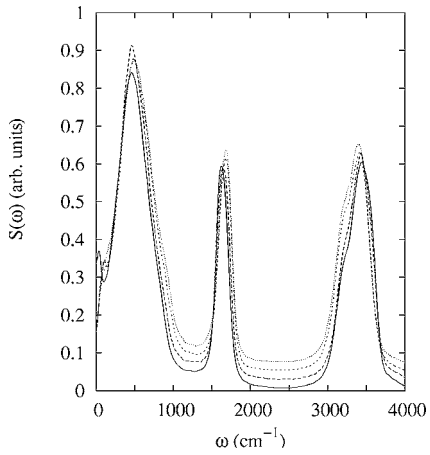

FIG. 6. Spectral densities obtained from our simulations at $T=398$ K. The curves have been displaced vertically for the sake of clarity. From bottom to top, we have bulk water density of 1 g/cm^3, and confined water between two graphite layers separated by 9, 12, and 15 Å. One observes that the bending peaks are moved forward while the stretching bands are basically unchanged with respect to bulk values.

spectral densities of oxygen atoms, and was not performed in this paper.

The position of the main bands in the spectral densities are given for four temperatures at Table I. From these data, we can say that the stretching bands are located at about the same position in all cases and for all temperatures, even though it is true that their frequency increases slightly when water is heated. The opposite happens with the bending peak: in confined water the maxima are located at higher frequencies than in bulk, but they slightly shift to lower wave numbers with temperature. There is no obvious trend in the changes of the rotation band: the differences in the values displayed in Table I are basically due to the numerical error of the procedure to find the spectra.

TABLE I. Frequency maxima (in cm^{-1}) for water confined between two graphite sheets. We also show the values corresponding to bulk water (density of 1 g/cm^3) at the same temperatures for comparison.

Temperature (K)	$\omega_{stretching}$	$\omega_{bending}$	$\omega_{rotation}$
	$z=9$ Å		
323	3400	1660	495
348	3420	1660	470
373	3420	1645	485
398	3430	1640	460
	$z=12$ Å		
323	3390	1685	485
348	3390	1685	480
373	3390	1680	485
398	3420	1680	485
	$z=15$ Å		
323	3395	1690	500
348	3400	1690	495
373	3395	1690	500
398	3400	1680	490
	Bulk		
323	3400	1635	495
348	3430	1645	485
373	3440	1620	475
398	3460	1620	455

TABLE II. Oxygen self-diffusion coefficients for all the systems and temperatures considered in this work. As before, the bulk data correspond to a density of 1 g/cm^3. All values are in 10^{-5} cm^2/s. Error bars are of the order of the last digit displayed.

Temperature (K)	D	D_z	D_{xy}
	$z=9$ Å		
323	1.8	~0	1.8
348	2.2	~0	2.2
373	2.8	~0	2.8
398	3.3	~0	3.3
	$z=12$ Å		
323	1.1	0.07	1.3
348	1.3	0.10	1.9
373	1.6	0.12	2.3
398	2.1	0.16	3.1
	$z=15$ Å		
323	0.7	0.11	1.0
348	1.0	0.13	1.4
373	1.3	0.18	1.9
398	1.4	0.22	2.0
	Bulk		
323	3.8		
348	6.0		
373	7.0		
398	8.5		

The remaining dynamical feature of these systems are their diffusion coefficients, already defined by means of Eq. (3). In Table II we show the results for the total self-diffusion coefficients of the three systems considered together with the bulk data for the same temperatures. Some features are immediately apparent. The D's in the direction perpendicular to the graphite sheets are appreciably lower than the ones in the xy planes. That means that the water molecules are basically confined to one layer in the z direction, irrespective of temperature. In addition the xy coefficients are appreciably lower than their bulk counterparts for all temperatures. In this, all three systems behave differently from their confined counterparts inside a carbon nanotube. In that last case, the water molecules move faster in the unconstrained direction than in the case of the bulk.[29] In any case, the magnitude of the coefficients indicates that, for the densities studied, we are still in the liquid zone, since solid total diffusion coefficients are of the order of 10^{-6} cm^2/s.

IV. CONCLUDING REMARKS

In this paper, we studied the high temperature behavior of water confined between two defectless graphite sheets of different separations. Phase diagrams are drawn up to 398 K and indicate the existence of a single stable phase in all graphite-graphite separations considered but the case of 9 Å. In this case, two well-defined phases at low temperature have been observed, corresponding to low and high density configurations. The characterization of the stable phases obtained has been performed by means of the calculations of some structural and dynamical properties of water under confinement. In the range of temperatures considered, and except for the diffusion coefficients, the changes in the studied properties are below 10%. In the case of diffusion, we observed a dramatic reduction of the water mobility when the liquid is restricted to quasi-two-dimensional geometries (for the separation of 9 Å at high density) and in all cases we found that diffusion in the direction normal to the graphite slabs is about one order of magnitude smaller than the overall diffusion.

ACKNOWLEDGMENTS

M.C.G. and J.M. gratefully acknowledge financial support from the "Ministerio de Educación y Ciencia" of Spain (Grant No. BFM2003-08211-C03-01). J.M. acknowledges financial support from "Generalitat de Catalunya" (Grant No. 2005SGR-00779) and from European Union FEDER funds (Grant No. UNPC-E015).

[1] C. Y. Lee, J. A. McCammon, and P. J. Rossky, J. Chem. Phys. **80**, 4448 (1984).
[2] S. B. Zhu and G. W. Robinson, J. Chem. Phys. **94**, 1403 (1990).
[3] A. Striolo, A. Chialvo, P. T. Cummings, and K. E. Gubbins, Langmuir **19**, 8583 (2003).
[4] K. Koga and H. Tanaka, J. Chem. Phys. **122**, 104711 (2005).
[5] M. Schoen and D. J. Diestler, J. Chem. Phys. **109**, 5596 (1998).
[6] M. C. Gordillo and J. Martí, J. Chem. Phys. **117**, 3425 (2002).
[7] P. Cabrera Sanfelix, S. Holloway, K. W. Kolasinski, and G. R. Darling, Surf. Sci. **532-535**, 166 (2003).
[8] A. Pertsin and M. Grunze, J. Phys. Chem. B **108**, 1357 (2004).
[9] R. Zangi, J. Phys.: Condens. Matter **16**, S5371 (2004).
[10] K. Lum, D. Chandler, and J. D. Weeks, J. Phys. Chem. B **103**, 4570 (1999).
[11] T. M. Truskett, P. G. Debenedetti, and S. Torquato, J. Chem. Phys. **114**, 2401 (2001).
[12] P. Kumar, S. V. Buldyrev, F. W. Starr, N. Giovambattista, and H. E. Stanley, Phys. Rev. E **72**, 051503 (2005).
[13] J. H. Walther, R. Jaffe, T. Halicioglu, and P. Koumoutsakos, J. Phys. Chem. B **105**, 9980 (2001).
[14] M. C. Gordillo and J. Martí, Chem. Phys. Lett. **329**, 341 (2000).
[15] P. Gallo, M. Rovere, and E. Spohr, Phys. Rev. Lett. **85**, 4317 (2000).
[16] P. Gallo, M. Rapinesi, and M. Rovere, J. Chem. Phys. **117**, 369 (2002).
[17] I. Brovchenko, A. Geiger, and A. Oleinikova, J. Chem. Phys. **120**, 1958 (2004).
[18] A. I. Kolesnikov, J. M. Zanotti, C. K. Loong, P. Thiyagarajan, A. P. Moravsky, R. O. Loutfy, and C. J. Burnham, Phys. Rev. Lett. **93**, 035503 (2004).
[19] M. V. Fernández-Serra and E. Artacho, Phys. Rev. Lett. **96**, 016404 (2006).
[20] M. C. Gordillo and J. Martí, Phys. Rev. B **67**, 205425 (2003).
[21] M. C. Gordillo, G. Nagy, and J. Martí, J. Chem. Phys. **123**, 054707 (2005).
[22] J. Martí, G. Nagy, M. C. Gordillo, and E. Guàrdia, J. Chem. Phys. **124**, 094703 (2006).
[23] J. Martí, J. A. Padró, and E. Guàrdia, J. Mol. Liq. **62**, 17 (1994).
[24] E. Spohr, J. Chem. Phys. **106**, 388 (1997).
[25] H. J. C. Berendsen, J. P. M. Postma, W. F. van Gunsteren, A. DiNola, and J. R. Haak, J. Chem. Phys. **81**, 3684 (1984).
[26] C. C. Liew, H. Inomata, and K. Arai, Fluid Phase Equilib. **144**, 287 (1998).
[27] J. Martí and M. C. Gordillo, Phys. Rev. B **63**, 165430 (2001).
[28] J. A. Padró and J. Martí, J. Chem. Phys. **120**, 1659 (2004).
[29] J. Martí and M. C. Gordillo, Phys. Rev. E **64**, 021504 (2001).